

Wave patterns generated by a supersonic moving body in a binary Bose-Einstein condensate

Yu. G. Gladush¹, A. M. Kamchatnov¹, Z. Shi², P. G. Kevrekidis², D. J. Frantzeskakis³, and B. A. Malomed⁴

¹ *Institute of Spectroscopy, Russian Academy of Sciences, Troitsk, Moscow Region, 142190, Russia*

² *Department of Mathematics and Statistics, University of Massachusetts, Amherst MA 01003-4515, USA*

³ *Department of Physics, University of Athens, Panepistimiopolis, Zografos, Athens 157 84, Greece*

⁴ *Department of Physical Electronics, Faculty of Engineering, Tel Aviv University, Tel Aviv 69978, Israel*

(Dated: November 2, 2018)

Generation of wave structures by a two-dimensional object (laser beam) moving in a two-dimensional two-component Bose-Einstein condensate with a velocity greater than both sound velocities of the mixture is studied by means of analytical methods and systematic simulations of the coupled Gross-Pitaevskii equations. The wave pattern features three regions separated by two Mach cones. Two branches of linear patterns similar to the so-called “ship waves” are located outside the corresponding Mach cones, and oblique dark solitons are found inside the wider cone. An analytical theory is developed for the linear patterns. A particular dark-soliton solution is also obtained, its stability is investigated, and two unstable modes of transverse perturbations are identified. It is shown that, for a sufficiently large flow velocity, this instability has a convective character in the reference frame attached to the moving body, which makes the dark soliton effectively stable. The analytical findings are corroborated by numerical simulations.

PACS numbers: 03.75.Kk

I. INTRODUCTION

Breakdown of superfluidity at large velocities of the flow is a fundamentally important problem which has been widely studied in physics of quantum liquids, such as ⁴He and Bose-Einstein condensates (BECs) of dilute atomic gases (see book [1] and references therein). As is known, the breakdown is caused by opening of channels of radiation of elementary excitations in the fluid, as it happens, for instance, with increase of the velocity of a body (“obstacle”) moving through the superfluid (in the experiment, a far-blue-detuned laser beam, which produces a local repulsive force acting on atoms, usually plays the role of the obstacle [2, 3]). In the BEC, solitary waves and vortices are readily generated if the size of the obstacle is of the order of (or greater than) the characteristic healing length of condensate. The generation of these structures manifests itself as an effective dissipation, which implies the loss of superfluidity at some critical value of the obstacle’s velocity [4, 5]. On the other hand, if the size of the obstacle is much smaller than the healing length, the main loss channel corresponds to the Cherenkov radiation of Bogoliubov excitations, and it opens at supersonic velocities of the obstacle [6]. If a large obstacle moves at a supersonic velocity, then the amplitude of the generated waves becomes large too. In the latter case, two dispersive shocks, which start their propagation from the front and the rear parts of the moving body, are formed. Far from the body, the shock front gradually transforms into a linear “ship wave” located outside the Mach cone [7, 8, 9, 10], whereas the rear zone of the shock is converted into a “fan” of oblique dark solitons located inside the Mach cone [11, 12, 13]. Although, as is well known, such dark solitons are unstable with respect to transverse perturbations, it was shown in [14] that for a flow velocity greater than some critical value this instability becomes a convective one (rather than being absolute) in the reference frame moving along with the obstacle. This fact actually means that the dark solitons are effectively stable in the region around the obstacle. Some of these structures have already been observed in experiments [7, 15], and similar non-stationary dispersive shocks were studied both theoretically and experimentally in BEC [2, 16, 17, 18, 19] (see also review [20]) and nonlinear optics [21, 22, 23, 24, 25, 26].

The picture described above corresponds to a single-component BEC whose mean-field dynamics is governed by the respective Gross-Pitaevskii equation [1]. At the same time, one of the focal points of activity in BEC physics has been the study of multi-component settings, a prototypical one being presented by binary mixtures [32, 33, 34]. These two-component media exhibit phase-separation phenomena [35, 36, 37] due to the nonlinear interaction between the different atomic species (or possibly different hyperfine states) that constitute the mixture. The formation of robust single- and multi-ring patterns [33, 38], the evolution of initially coincident triangular vortex lattices through a turbulent regime into an interlaced square vortex lattice [39] in coupled hyperfine states in the ⁸⁷Rb condensate, and the study of the interplay between atomic states at different Zeeman levels in the ²³Na condensate, forming striated magnetic domains in optical traps [40, 41], are only a small subset among the many possibilities that multi-component BECs can offer. It should also be noted that mixtures with a higher number of components, namely spinor condensates [42, 43], are known too. They have been realized with the help of far-off-resonant optical techniques for trapping ultracold atomic gases [44], which, in turn, allowed the spin degree of freedom to be explored (previously, it

was frozen in magnetic traps).

Our aim in the present work is to unite these two areas by investigating the effects generated by the motion of an obstacle in a “pancake”-shaped, i.e., effectively two-dimensional (2D), *two-component* BEC. In an earlier work [45], the critical situation, when the obstacle had the velocity comparable to the two speeds of sound in the two-component system, was examined. Here, we extend the analysis to the supercritical case, when the speed of the moving body may be significantly higher than the sound speed(s). We demonstrate that two branches of linear, so-called “ship-wave”, patterns form outside of the two Mach cones (which are associated with the speeds of sound), while oblique dark solitons are located inside the wider Mach cone. While these dark solitons are unstable at relatively low velocities of the motion of the obstacle, they can be convectively stabilized at sufficiently high values of the velocity.

The presentation is structured as follows. In section II, we outline the model under consideration. In section III, we study the linear (ship) waves by means of both analytically and numerical methods. In section IV, we study dark solitons (again, by dint of both analytical and numerical methods). Finally, we summarize our findings in section V, and discuss potential directions for future work.

II. MATHEMATICAL MODEL AND SETUP

In the usual mean-field approximation, the 2D flow of a binary condensate mixture past an obstacle obeys the system of nonlinearly coupled Gross-Pitaevskii equations (GPEs), with spatial coordinates $\mathbf{r} = (x, y)$. In the scaled form, the equations take a well-known form [1, 20],

$$\begin{aligned} i\frac{\partial\psi_1}{\partial t} &= -\frac{1}{2}\Delta\psi_1 + (g_{11}|\psi_1|^2 + g_{12}|\psi_2|^2)\psi_1 + V(\mathbf{r}, t)\psi_1, \\ i\frac{\partial\psi_2}{\partial t} &= -\frac{1}{2}\Delta\psi_2 + (g_{12}|\psi_1|^2 + g_{22}|\psi_2|^2)\psi_2 + V(\mathbf{r}, t)\psi_2. \end{aligned} \quad (1)$$

We assume that atoms in both species have the same mass (i.e., they represent different hyperfine states of the same atom, as is often the case, see e.g., Ref. [38] and references therein), $V(\mathbf{r}, t)$ being the potential induced by the moving obstacle, which is identical for both components.

Small-amplitude waves and solitons correspond to potential flows with zero vorticity, for which Eqs. (1) can be transformed into a hydrodynamic form by means of substitutions

$$\psi_1(\mathbf{r}, t) = \sqrt{n_1(\mathbf{r}, t)} \exp\left(i \int^{\mathbf{r}} \mathbf{u}_1(\mathbf{r}', t) d\mathbf{r}' - i\mu_1 t\right), \quad \psi_2(\mathbf{r}, t) = \sqrt{n_2(\mathbf{r}, t)} \exp\left(i \int^{\mathbf{r}} \mathbf{u}_2(\mathbf{r}', t) d\mathbf{r}' - i\mu_2 t\right), \quad (2)$$

where $n_{1,2}(\mathbf{r}, t)$ are the atom densities of the two BEC components, $\mathbf{u}_{1,2}(\mathbf{r}, t)$ their velocity fields, and $\mu_{1,2}$ the respective chemical potentials. Substituting Eqs. (2) into the Eqs. (1) we arrive at the following system,

$$\begin{aligned} n_{1,t} + \nabla \cdot (n_1 \mathbf{u}_1) &= 0, & n_{2,t} + \nabla \cdot (n_2 \mathbf{u}_2) &= 0, \\ \mathbf{u}_{1,t} + (\mathbf{u}_1 \cdot \nabla) \mathbf{u}_1 + g_{11} \nabla n_1 + g_{12} \nabla n_2 + \nabla \left(\frac{(\nabla n_1)^2}{8n_1^2} - \frac{\Delta n_1}{4n_1} \right) + \nabla V(\mathbf{r}, t) &= 0, \\ \mathbf{u}_{2,t} + (\mathbf{u}_2 \cdot \nabla) \mathbf{u}_2 + g_{12} \nabla n_1 + g_{22} \nabla n_2 + \nabla \left(\frac{(\nabla n_2)^2}{8n_2^2} - \frac{\Delta n_2}{4n_2} \right) + \nabla V(\mathbf{r}, t) &= 0. \end{aligned} \quad (3)$$

The first pair of the equations represents the conservation of the number of atoms in each component, and the second pair corresponds to the Euler’s equations for fluid velocities under the action of the pressure induced by interactions between atoms, the obstacle’s potential, and quantum dispersion.

We consider waves generated by the obstacle moving at constant velocity U along the x -axis,

$$V(\mathbf{r}, t) = V(x - Ut), \quad (4)$$

through a uniform condensate, so that at $|x| \rightarrow \infty$ both components have constant densities and vanishing velocities. This setting implies the absence of a trapping potential in the plane of the quasi-2D BEC (or, more realistically, a very weak trapping). In the reference frame moving along with the obstacle, the unperturbed condensate flows at constant velocity $\mathbf{u} = (-U, 0)$, hence the respective boundary conditions for the densities and velocities are

$$n_1 \rightarrow n_{10}, \quad n_2 \rightarrow n_{20}, \quad \mathbf{u}_1 \rightarrow \mathbf{u}, \quad \mathbf{u}_2 \rightarrow \mathbf{u} \quad \text{at} \quad |x| \rightarrow \infty. \quad (5)$$

As follows from Eqs. (5), chemical potentials $\mu_{1,2}$ are related with the asymptotic densities n_{10}, n_{20} by the relations

$$\mu_1 = g_{11}n_{10} + g_{12}n_{20}, \quad \mu_2 = g_{12}n_{10} + g_{22}n_{20}. \quad (6)$$

In this reference frame, the wave pattern is a stationary one, which is convenient for analytical considerations.

III. LINEAR “SHIP WAVES”

We first aim to consider linear waves generated by the moving obstacle, assume that potential $V(\mathbf{r}, t)$ is weak enough to apply the perturbation theory [6] based on linearized equations. Actually, the approximation is valid everywhere where the amplitude of the waves is small—in particular, far enough from the obstacle outside the Mach cones associated with the speeds of sound. Thus, we introduce small deviations from the uniform state, namely,

$$n_1 = n_{10} + n'_1, \quad n_2 = n_{20} + n'_2, \quad \mathbf{u}_1 = \mathbf{u} + \mathbf{u}'_1, \quad \mathbf{u}_2 = \mathbf{u} + \mathbf{u}'_2, \quad (7)$$

and accordingly linearize Eqs. (3):

$$n'_{1,t} + n_{10}(\nabla \cdot \mathbf{u}'_1) + (\mathbf{u} \cdot \nabla)n'_1 = 0, \quad n'_{2,t} + n_{20}(\nabla \cdot \mathbf{u}'_2) + (\mathbf{u} \cdot \nabla)n'_2 = 0, \quad (8)$$

$$\mathbf{u}'_{1,t} + (\mathbf{u} \cdot \nabla)\mathbf{u}'_1 + g_{11}\nabla n'_1 + g_{12}\nabla n'_2 - \frac{1}{4n_{10}}\nabla(\Delta n'_1) = -\nabla V, \quad (9)$$

$$\mathbf{u}'_{2,t} + (\mathbf{u} \cdot \nabla)\mathbf{u}'_2 + g_{12}\nabla n'_1 + g_{22}\nabla n'_2 - \frac{1}{4n_{20}}\nabla(\Delta n'_2) = -\nabla V.$$

In the stationary case, all time derivatives vanish. Further, we apply the Fourier transform,

$$n'_1(\mathbf{r}, t) = \int \int \tilde{n}'_1(\mathbf{k}, t) e^{i\mathbf{k}\mathbf{r}} \frac{d^2k}{(2\pi)^2}. \quad (10)$$

Then, we eliminate the velocity perturbations in Eqs. (9) in favor of the densities, arriving at the following system of two linear equations:

$$\begin{aligned} [-(\mathbf{k} \cdot \mathbf{u})^2 + k^2(g_{11}n_{10} + k^2/4)]\tilde{n}'_1 + k^2g_{12}n_{10}\tilde{n}'_2 &= -k^2\tilde{V}n_{10}, \\ k^2g_{12}n_{20}\tilde{n}'_1 + [-(\mathbf{k} \cdot \mathbf{u})^2 + k^2(g_{22}n_{20} + k^2/4)]\tilde{n}'_2 &= -k^2\tilde{V}n_{20}, \end{aligned} \quad (11)$$

where tildes denote the Fourier components. This linear system can be readily solved for $\tilde{n}'_{1,2}$ and the inverse Fourier transform yields

$$\begin{aligned} n'_1 &= -n_{10} \int \int \frac{k^2\tilde{V} \{ [-(\mathbf{k} \cdot \mathbf{u})^2 + k^2(g_{22}n_{20} + k^2/4)] - k^2g_{12}n_{20} \}}{((\mathbf{k} \cdot \mathbf{u})^2 - \omega_+^2)((\mathbf{k} \cdot \mathbf{u})^2 - \omega_-^2)} \frac{d^2k}{(2\pi)^2}, \\ n'_2 &= -n_{20} \int \int \frac{k^2\tilde{V} \{ [-(\mathbf{k} \cdot \mathbf{u})^2 + k^2(g_{11}n_{10} + k^2/4)] - k^2g_{12}n_{10} \}}{((\mathbf{k} \cdot \mathbf{u})^2 - \omega_+^2)((\mathbf{k} \cdot \mathbf{u})^2 - \omega_-^2)} \frac{d^2k}{(2\pi)^2}, \end{aligned} \quad (12)$$

where the dispersion relations for the linear waves in the binary mixture are given by

$$\omega_{\pm}^2 = \frac{1}{2}k^2 \left[g_{11}n_{10} + g_{22}n_{20} + \frac{1}{2}k^2 \pm \sqrt{(g_{11}n_{10} - g_{22}n_{20})^2 + 4g_{12}^2n_{10}n_{20}} \right], \quad (13)$$

In the long-wave limit, Eqs. (13) yield the sound velocities [45], $c_{\pm} = \omega(k)/k$, given by:

$$c_{\pm} \equiv \lim_{k \rightarrow 0} \frac{\omega(k)}{k} = \sqrt{\frac{g_{11}n_{10} + g_{22}n_{20} \pm \sqrt{(g_{11}n_{10} - g_{22}n_{20})^2 + 4g_{12}^2n_{10}n_{20}}}{2}}. \quad (14)$$

Expressions (12) can be analyzed following the lines of Ref. [9, 10]. To this end, we introduce new coordinates (see Fig. 1),

$$\mathbf{r} \equiv (-r \cos \chi, r \sin \chi), \quad \mathbf{k} \equiv (k \cos \eta, k \sin \eta), \quad (15)$$

and assume that the wavelength of the pattern is much greater than the characteristic size of the obstacle, hence its potential can be approximated by the form $V(\mathbf{r}) = V_0\delta(\mathbf{r})$. Then, we obtain

$$\begin{aligned} n'_1 &= \frac{4V_0n_{10}}{\pi^2} \int_{-\pi}^{\pi} \int_0^{\infty} \frac{k[(g_{22} - g_{12})n_{20} + k^2/4 - U^2 \cos^2 \eta] e^{i\mathbf{k}\mathbf{r}}}{(k^2 - k_+^2 - i0)(k^2 - k_-^2 - i0)} dk d\eta, \\ n'_2 &= \frac{4V_0n_{20}}{\pi^2} \int_{-\pi}^{\pi} \int_0^{\infty} \frac{k[(g_{11} - g_{12})n_{10} + k^2/4 - U^2 \cos^2 \eta] e^{i\mathbf{k}\mathbf{r}}}{(k^2 - k_+^2 - i0)(k^2 - k_-^2 - i0)} dk d\eta, \end{aligned} \quad (16)$$

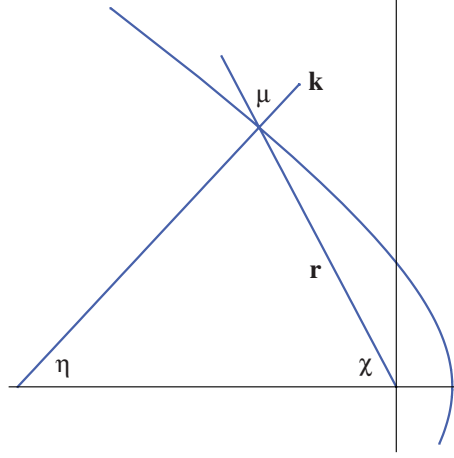


FIG. 1: (Color online.) Coordinates defining radius-vector \mathbf{r} and wave vector \mathbf{k} . The latter one is normal to the wave front of one of the ship-wave modes, which is shown schematically by a curve.

where infinitesimal imaginary parts in the denominators are written to define correct contributions from the poles corresponding to adiabatically slow switching on of the potential, and

$$k_{\pm} \equiv 2\sqrt{U^2 \cos^2 \eta - c_{\pm}^2}. \quad (17)$$

Next, we split the integration domain of η into two parts: $\int_{-\pi/2}^{3\pi/2} d\eta \equiv \int_{-\pi/2}^{\pi/2} d\eta + \int_{\pi/2}^{3\pi/2} d\eta$. After replacement $\eta' = \eta - \pi$ in the second term, one can notice that the integrand turns into its own complex conjugate, allowing one to write the integrals in Eq. (16) as

$$\begin{aligned} n'_1 &= \frac{8V_0 n_{10}}{\pi^2} \text{Re} \int_{-\pi/2}^{\pi/2} d\eta \int_0^{\infty} \frac{k[(g_{22} - g_{12})n_{20} + k^2/4 - U^2 \cos^2 \eta] e^{i\mathbf{k}\mathbf{r}}}{(k^2 - k_+^2 - i0)(k^2 - k_-^2 - i0)} dk, \\ n'_2 &= \frac{8V_0 n_{20}}{\pi^2} \text{Re} \int_{-\pi/2}^{\pi/2} d\eta \int_0^{\infty} \frac{k[(g_{11} - g_{12})n_{10} + k^2/4 - U^2 \cos^2 \eta] e^{i\mathbf{k}\mathbf{r}}}{(k^2 - k_+^2 - i0)(k^2 - k_-^2 - i0)} dk. \end{aligned} \quad (18)$$

The integration over k should be carried out over the positive real half-axis. However, we can add to this path a quarter of an infinite circle and the imaginary half-axis in the complex k plane, to build a closed integration contour. It is easy to show that the contribution from the quarter of the infinite circle is zero, and contribution from the imaginary axis depends on r as r^{-2} , decaying at large r much faster than the contribution of the pole, which is $\sim r^{-1/2}$. Thus, far from the obstacle, it is sufficient to keep only the contribution from the poles, which yields ($\nu \equiv \pi - \chi - \eta$)

$$\begin{aligned} n'_1 &= -\frac{2V_0 n_{10}}{\pi(c_+^2 - c_-^2)} \left\{ [c_+^2 - (g_{22} - g_{12})n_{20}] \text{Im} \int_{-\pi/2}^{\pi/2} d\eta e^{ik_+ r \cos \nu} - [c_-^2 - (g_{22} - g_{12})n_{20}] \text{Im} \int_{-\pi/2}^{\pi/2} d\eta e^{ik_- r \cos \nu} \right\}, \\ n'_2 &= -\frac{2V_0 n_{20}}{\pi(c_+^2 - c_-^2)} \left\{ [c_+^2 - (g_{11} - g_{12})n_{10}] \text{Im} \int_{-\pi/2}^{\pi/2} d\eta e^{ik_+ r \cos \nu} - [c_-^2 - (g_{11} - g_{12})n_{10}] \text{Im} \int_{-\pi/2}^{\pi/2} d\eta e^{ik_- r \cos \nu} \right\}. \end{aligned} \quad (19)$$

Far from the obstacle, where phases $\mathbf{k}_{\pm} \mathbf{r} = r s_{\pm}$ are large, we are dealing with large values of

$$s_{\pm}(\eta) = k_{\pm}(\eta) \cos(\chi + \eta), \quad (20)$$

and the integrals in Eq. (19) can be estimated by means of the standard stationary-phase method. Since calculations of both integrals are identical, we consider, for definiteness, the integral over k_+ . Condition $\partial s_+ / \partial \eta = 0$ is an equation for the stationary-phase point, which can be easily transformed to

$$\tan \nu_+ = (2U^2/k_+^2) \sin 2\eta_+, \quad (21)$$

or, with regard to the definition of ν , we obtain an expression for χ ,

$$\tan \chi_+ = \frac{(1 + k_+^2/(2c_+^2)) \tan \eta_+}{U^2/c_+^2 - (1 + k_+^2/(2c_+^2))}. \quad (22)$$

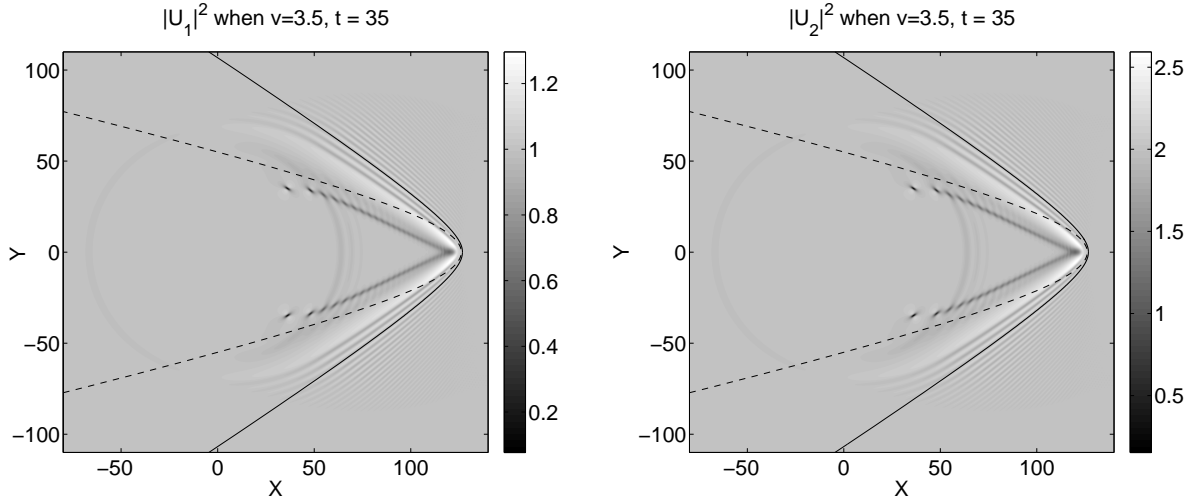


FIG. 2: Spatial contour plots of densities of the two components (left and right panels, respectively) of the BEC for the flow velocity $U = 3.5$, at $t = 35$. The form of the obstacle's potential used in this case is $V(x, y, t) = 2 \left[\text{sech} \left(\frac{\sqrt{(x - Ut)^2 + y^2}}{2} \right) \right]^2$. Solid and dashed thin lines correspond to wave crests of two modes of ship waves.

Here η_+ takes values in interval

$$-\arccos \frac{1}{M_+} \leq \eta_+ \leq \arccos \frac{1}{M_+}, \quad M_+ \equiv \frac{U}{c_+}, \quad (23)$$

while the corresponding vector $\{x, y\}$, given by the parametric expressions,

$$x(\eta_+) = \frac{4\phi c_+^2}{k_+^3} (M_+^2 \cos 2\eta_+ - 1) \cos \eta_+, \quad y(\eta_+) = \frac{4\phi c_+^2}{k_+^3} (2M_+^2 \cos^2 \eta_+ - 1) \sin \eta_+, \quad (24)$$

moves along a curve with constant phase ϕ (e.g., a crest line).

As usual in the method of stationary phase, we reduce the integrals in (19) to Gaussian ones and, as a final result, obtain

$$\begin{aligned} n'_1 = & -\frac{2V_0 n_{10}}{\pi(c_+^2 - c_-^2)} \left\{ [c_+^2 - (g_{22} - g_{12})n_{20}] \sqrt{\frac{2\pi}{k_+ r}} \right. \\ & \times \frac{[1 + (4U^2/k_+^2) \sin^2(2\eta_+)]^{1/4}}{[1 + (4U^2/k_+^2) \cos 2\eta_+ + (12U^4/k_+^4) \sin^2(2\eta_+)]^{1/2}} \cos(k_+ r \cos \nu_+ - \pi/4) \\ & - [c_-^2 - (g_{22} - g_{12})n_{20}] \sqrt{\frac{2\pi}{k_- r}} \frac{(1 + (4U^2/k_-^2) \sin^2 2\eta_-)^{1/4}}{[1 + (4U^2/k_-^2) \cos(2\eta_-) + (12U^4/k_-^4) \sin^2(2\eta_-)]^{1/2}} \\ & \left. \times \cos(k_- r \cos \nu_- - \pi/4) \right\} \quad (25) \end{aligned}$$

where $\nu_{\pm} \equiv \pi - \chi_{\pm} - \eta_{\pm}$, and similar expressions can be derived for the density oscillations of the second component of the binary condensate.

An example of wave patterns generated by numerical simulations of Eqs. (1) is displayed in Fig. 2, for parameters $g_{11} = 1.5$, $g_{22} = 1.25$, $g_{12} = 1.0$, and $n_{10} = 1.0$, $n_{20} = 2.0$ and velocity $U = 3.5$. Three different types of waves can clearly be distinguished in this picture. First, one observes ship waves outside the Mach cones, which were analyzed above. Oblique dark solitons, which are located inside the outer Mach cone, they will be discussed in the next Section. One can also note that the oblique solitons are modulated by concentric circular waves, which were actually generated by the initial introduction (switching on) of the obstacle's potential. These circular waves are not related to the steady regime and will not be considered here.

We have compared analytical results (24) for the crest lines with the numerical findings. The analytically predicted curves are shown by thin solid and dashed lines in Fig. 2. To simplify the pattern, we have chosen the parameters of the binary BEC so that the chemical potentials (6) of both components are equal to each other. As a result, the smaller sound velocity satisfies the relation $c_-^2 = (g_{11} - g_{12})n_{10} = (g_{22} - g_{12})n_{20}$ and hence the last term in Eq. (25) as well as in analogous expression for n'_2 vanishes. Therefore the ship waves in the region between the two Mach cones are not visible in agreement with the results of numerical simulations. Another linear mode describes the ship waves outside of the outer Mach cone, and the analytically calculated form of the crest line demonstrates excellent agreement with the numerically obtained one.

IV. OBLIQUE DARK SOLITONS

As mentioned above, in Fig. 2 one can observe oblique dark solitons located inside the outer Mach cone. It is worthy to note that they decay into vortices at end points, which is a result of the “snaking” instability of dark soliton stripes in 2D [27, 28, 29] (see also [46]). However, for large velocities U this instability is convective only [14], which means that the dark solitons are effectively stable around the obstacle and, hence, the length of the dark solitons increases with time. The solitons originate from a depression in the density distribution formed behind the obstacle by the flow, therefore their depth also varies near the obstacle. However, upon sufficiently long evolution time, there exists a region where the oblique dark solitons can be considered as quasi-stationary structures. In this region, the solitons are described by the stationary solution of the GPEs. This allows us to take the stationary GPEs in the hydrodynamic form (3),

$$\begin{aligned} \nabla \cdot (n_1 \mathbf{u}_1) &= 0, & \nabla \cdot (n_2 \mathbf{u}_2) &= 0, \\ (\mathbf{u}_1 \cdot \nabla) \mathbf{u}_1 + g_{11} \nabla n_1 + g_{12} \nabla n_2 + \nabla \left(\frac{(\nabla n_1)^2}{8n_1^2} - \frac{\Delta n_1}{4n_1} \right) &= 0, \\ (\mathbf{u}_2 \cdot \nabla) \mathbf{u}_2 + g_{12} \nabla n_1 + g_{22} \nabla n_2 + \nabla \left(\frac{(\nabla n_2)^2}{8n_2^2} - \frac{\Delta n_2}{4n_2} \right) &= 0. \end{aligned} \quad (26)$$

Here, it is also taken into regard that the obstacle’s potential is negligible far from it. Equations (26) should be solved with the boundary conditions

$$n_1 \rightarrow n_{10}, \quad n_2 \rightarrow n_{20}, \quad \mathbf{u}_1 \rightarrow (-U, 0), \quad \mathbf{u}_2 \rightarrow (-U, 0) \quad \text{at} \quad |x| \rightarrow \infty, \quad (27)$$

where $-U$ is the common velocity of both components relative to the obstacle. Under the assumption that the solution depends only on

$$\xi = \frac{x - ay}{\sqrt{1 + a^2}}, \quad (28)$$

where a determines the slope of the oblique dark soliton, this system can be readily reduced to equations

$$\begin{aligned} \frac{1}{8}(n_{1,\xi}^2 - 2n_1 n_{1,\xi\xi}) + g_{11} n_1^3 + g_{12} n_1^2 n_2 + \frac{1}{2} q n_{10}^2 - (\frac{1}{2} q + \mu_1) n_1^2 &= 0, \\ \frac{1}{8}(n_{2,\xi}^2 - 2n_2 n_{2,\xi\xi}) + g_{12} n_1 n_2^2 + g_{22} n_2^3 + \frac{1}{2} q n_{20}^2 - (\frac{1}{2} q + \mu_2) n_2^2 &= 0, \end{aligned} \quad (29)$$

where μ_1 and μ_2 are the chemical potentials defined above in Eq. (6), and

$$q \equiv \frac{U^2}{1 + a^2}. \quad (30)$$

The flow velocities are related to the densities as follows:

$$\mathbf{u}_i = \left(\frac{(n_{i0} + a^2 n_i) U}{(1 + a^2) n_i}, -\frac{a U (n_{i0} - n_i)}{(1 + a^2) n_i} \right), \quad i = 1, 2. \quad (31)$$

In general, system (29) has to be solved numerically. However, if the chemical potentials of the two components are equal,

$$\mu_1 = \mu_2 = \mu, \quad (32)$$

the system admits a simple analytical solution in a closed form. In this case, we look for the solution as $n_1 = n_{10}f(\xi)$, $n_2 = n_{20}f(\xi)$, reducing both equations (29) to a single one,

$$\frac{1}{8}(f_\xi^2 - 2ff_{\xi\xi}) + \mu f^3 + \frac{1}{2}q - (\frac{1}{2}q + \mu)f^2 = 0. \quad (33)$$

Dark-soliton solutions to Eq. (33) are known [12]:

$$n_1 = n_{1s} = n_{10}f(\xi), \quad n_2 = n_{2s} = n_{20}f(\xi), \quad f(\xi) = 1 - \frac{1 - q/c_+^2}{\cosh^2 \left[\sqrt{c_+^2 - q} (x - ay) / \sqrt{1 + a^2} \right]}, \quad (34)$$

where we have also taken into regard that condition (32) leads to the following expressions for the sound velocities (for definiteness, we suppose here that $g_{11}, g_{22} > g_{12}$, i.e., the inter-species repulsion is weaker than the repulsive self-interactions of the two components):

$$c_-^2 = (g_{11} - g_{12})n_{10}, \quad c_+^2 = \mu. \quad (35)$$

Obviously, solution (34) exists if the condition $q < c_+^2$ is satisfied. If we introduce angle θ between the direction of the flow and the orientation of the dark-soliton stripe, so that $a = \cot \theta$, the latter condition can be transformed into

$$\sin^2 \theta < \frac{c_+^2}{U^2} = \frac{1}{M_+^2}, \quad M_+ \equiv \frac{U}{c_+}. \quad (36)$$

Thus, the soliton must be located inside the outer Mach cone, which is defined by the equation

$$\sin \theta_+ = \frac{1}{M_+}. \quad (37)$$

Although we have arrived at this conclusion under assumption (32), we conjecture that it is correct too in the general case of unequal chemical potentials, which is confirmed by the fact that our numerical simulations always produced oblique solitons confined inside the outer Mach cone. The respective numerically generated profiles of the densities are shown in Fig. 3 as a function of y at a fixed value of x ; the corresponding phase profiles are also shown in the figure. It is observed that the oblique solitons are indeed located inside the outer Mach cone [as defined by Eq. (37)] but outside of the inner cone, which is defined by $\sin \theta_- = 1/M_-$. Profiles of the solitons' densities are close to the analytically predicted ones and the jumps of phases are also in agreement with the expected dark-soliton behavior.

According to condition (36), solution (34) exists for any supersonic flow with $U > c_+$, the same being true for the existence of numerical solutions to system (29) in the general case, $\mu_1 \neq \mu_2$. However, that does not mean that the oblique dark solitons can be generated by any such flow. While the numerical results presented in Fig. 2 show that oblique solitons indeed exist for velocity $U = 3.5$, the opposite situation, when oblique dark solitons do not emerge, is presented in Fig. 4 by means of density patterns which correspond to a lower supersonic flow velocity, $U = 1.2$. It is seen that vortex streets are generated in the latter case, rather than dark solitons. Such a behavior is related to the well-known instability of dark solitons with respect to transverse perturbations [27, 28, 29]. The instability splits dark solitons into vortex-antivortex pairs, hence dark solitons cannot develop from the density depression behind the obstacle moving at a relatively low velocity. However, the numerical simulations presented in Fig. 2 indicate that the oblique solitons become effectively stable if the flow velocity is sufficiently high, as first was noticed in Ref. [12] for the case of a one-component BEC. The stabilization was explained in Ref. [14] as a transition from the absolute instability of dark solitons to their convective instability, at some critical value of the flow velocity, $U_{cr} \geq c_+$, so that the unstable disturbances are carried away by the flow from the region around the obstacle where, as a result, the dark solitons look as effectively stable objects. Here, we aim to consider such a stabilization transition for the case of the two-component BEC, which features two unstable modes of perturbations around the dark soliton.

To find the spectrum of small-amplitude linear waves propagating along the soliton, we now consider this solution in the reference frame in which the condensate has zero velocity far from the obstacle. To this end, we rotate the coordinate system by angle $\varphi = \arctan a$ [recall a determines the orientation of the dark soliton, according to Eq. (28)], and perform the Galilean transformation to the frame moving relative to the obstacle at velocity $(U \cos \varphi, U \sin \varphi)$:

$$\begin{aligned} \tilde{x} &= x \cos \varphi - y \sin \varphi - U \cos \varphi \cdot t, \\ \tilde{y} &= x \sin \varphi + y \cos \varphi - U \sin \varphi \cdot t. \end{aligned} \quad (38)$$

After the transformation, velocity fields (31) become

$$\tilde{\mathbf{u}}_1 = (v(n_{10}/n_{1s} - 1), 0), \quad \tilde{\mathbf{u}}_2 = (v(n_{20}/n_{2s} - 1), 0), \quad (39)$$

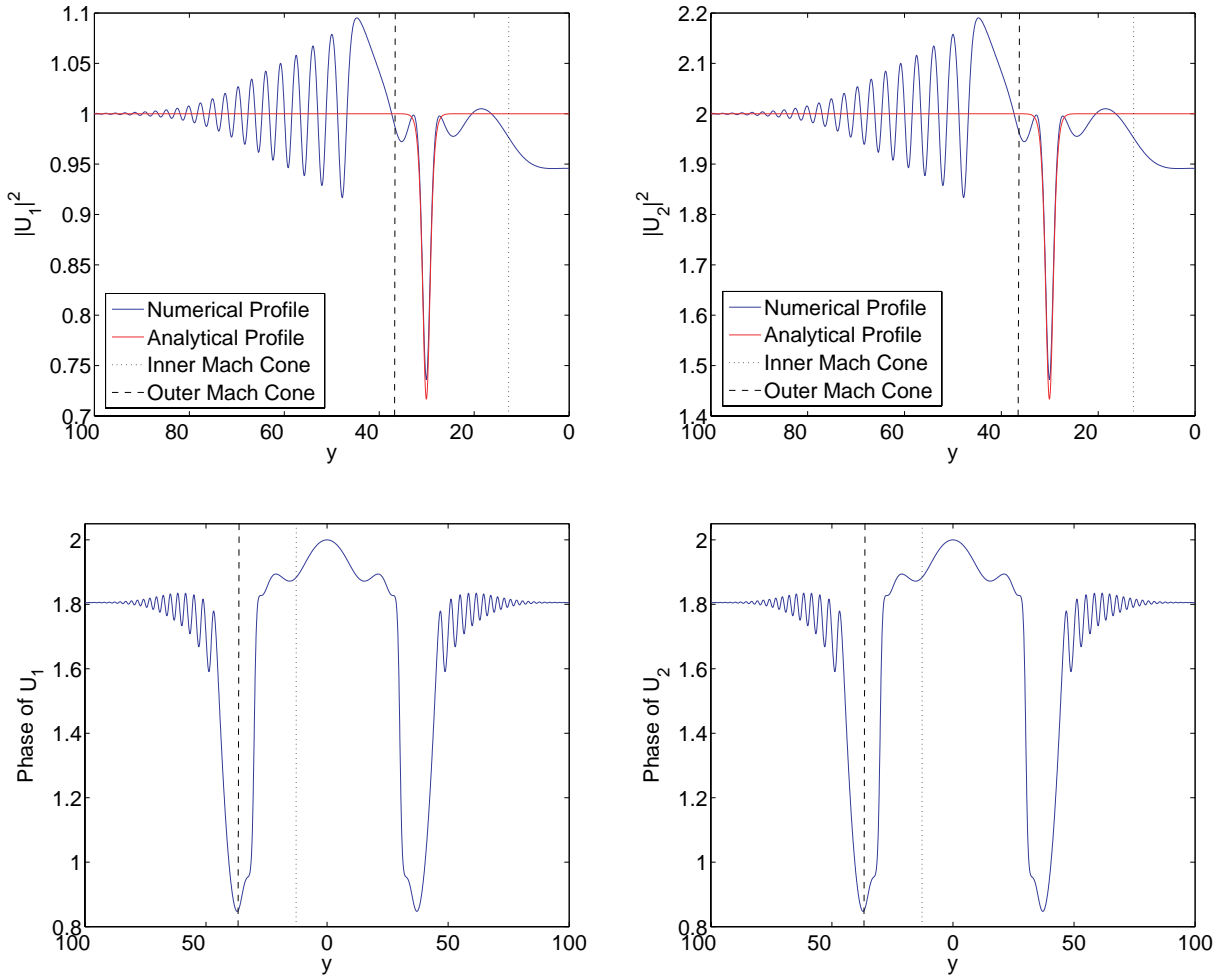


FIG. 3: (Color online.) Plots of densities (top) and phases (bottom) of the two BEC components for flow velocity $U = 4.5$. The positions of the Mach cones are shown by dashed lines, making it evident that the oblique dark solitons are located inside the outer Mach cone, in agreement with Eq. (36). The chemical potentials are $\mu_1 = \mu_2 = 3.5$, cf. Eq. (32), and the configurations are shown at $t = 30$.

and the densities take the form of

$$\begin{aligned} \tilde{n}_{1s} &= n_{10}f(\zeta), & \tilde{n}_{2s} &= n_{20}f(\zeta), \\ f(\zeta) &= 1 - \frac{1 - v^2/c_+^2}{\cosh^2 \left[\sqrt{c_+^2 - v^2} \zeta \right]}, & \zeta &= \tilde{x} - vt, \end{aligned} \quad (40)$$

where the soliton's velocity in the new reference frame is

$$v = \frac{U}{\sqrt{1 + a^2}}. \quad (41)$$

Below, we omit tildes attached to the new variables.

We take small transverse perturbations of the dark-soliton solution as

$$\begin{aligned} \psi_1 &= \psi_{1s}(\zeta) + (\psi'_1 + i\psi''_1) \exp(i\phi_{1s}(\zeta) - i\mu_1 t), \\ \psi_2 &= \psi_{2s}(\zeta) + (\psi'_2 + i\psi''_2) \exp(i\phi_{2s}(\zeta) - i\mu_2 t), \end{aligned} \quad (42)$$

where the unperturbed solution depends only on $\zeta = x - vt$,

$$\psi_{js} = \sqrt{n_{js}} \exp(i\phi_{js}(\zeta) - i\mu_j t), \quad (43)$$

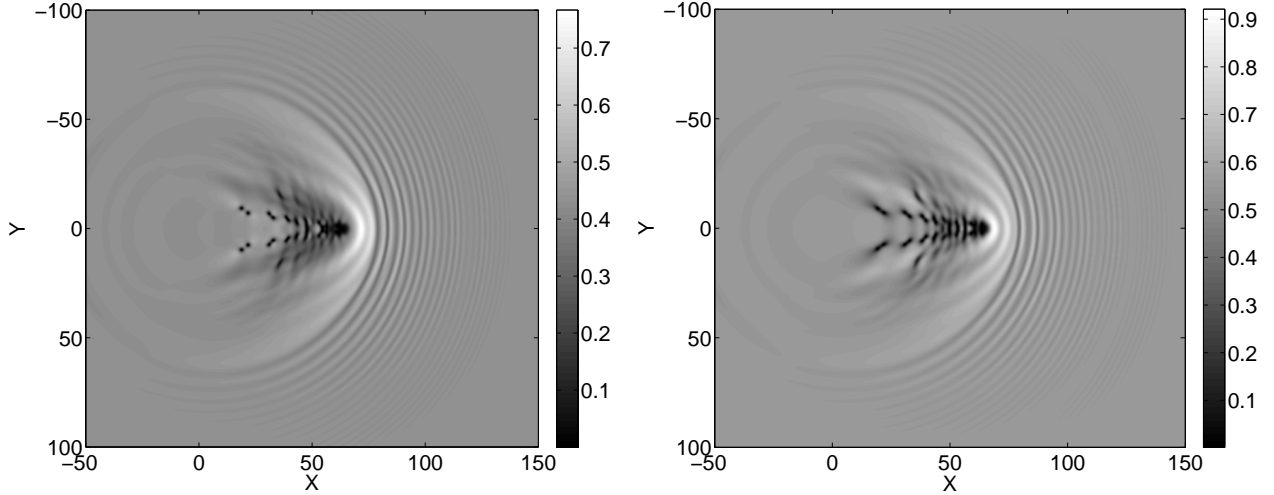


FIG. 4: Plots of densities of two BEC components for flow velocity $U = 1.2$ at $t = 55$.

and phases ϕ_{js} are related to the densities by equations

$$\frac{\partial \phi_{js}}{\partial \zeta} = v \left(\frac{n_{j0}}{n_{js}} - 1 \right). \quad (44)$$

Perturbations ψ' and $i\psi''$ depend on y and t as $\exp(ipy + \Gamma t)$. Substitution of expressions (42) into Eqs. (1) and the linearization with respect to ψ' and $i\psi''$ lead to an eigenvalue problem,

$$\begin{pmatrix} A_1 & -L_{I1} & 0 & 0 \\ L_{R1} & A_1 & B & 0 \\ 0 & 0 & A_2 & -L_{I2} \\ B & 0 & L_{R2} & A_2 \end{pmatrix} \begin{pmatrix} \psi'_1 \\ \psi''_1 \\ \psi'_2 \\ \psi''_2 \end{pmatrix} = \Gamma \begin{pmatrix} \psi'_1 \\ \psi''_1 \\ \psi'_2 \\ \psi''_2 \end{pmatrix}, \quad (45)$$

$$\begin{aligned} A_j &\equiv \frac{vn_{j0}n_{js,\zeta}}{2n_{js}^2} - \frac{vn_{j0}}{n_{js}} \frac{\partial}{\partial \zeta}, \\ B &\equiv -2g_{12}\sqrt{n_{1s}n_{2s}}, \\ L_{Ij} &\equiv \frac{1}{2} \frac{\partial^2}{\partial \zeta^2} - \frac{1}{2} \frac{n_{j0}v^2}{n_{js}^2} + \frac{1}{2}(v^2 - p^2) - g_{jj}n_{js} - g_{lj}n_{ls} + \mu_j, \\ L_{Rj} &\equiv \frac{1}{2} \frac{\partial^2}{\partial \zeta^2} - \frac{1}{2} \frac{n_{j0}v^2}{n_{js}^2} + \frac{1}{2}(v^2 - p^2) - 3g_{jj}n_{js} - g_{lj}n_{ls} + \mu_j, \\ &j = 1, 2, \quad l = 1, 2, \quad l \neq j. \end{aligned} \quad (46)$$

System (45) determines the growth rates $\Gamma_{1,2}(p)$ of small perturbations traveling along the dark-soliton's crest. The result is the presence of two unstable branches, examples of which are shown in Fig. 5. As one can see, both branches indeed feature regions of wave vector p with $\text{Re } \Gamma(p) > 0$. The transition to convective instability should be considered separately for each branch.

Returning to the reference system attached to the moving obstacle, we get dispersion relations

$$\omega_{1,2}(p) = U_s p + i\Gamma(p, v), \quad (47)$$

where $U_s = v \sin \varphi \equiv aU/\sqrt{1+a^2}$ is the component of the flow velocity along the dark soliton. The perturbations may be represented as Fourier integrals over linear modes obeying dispersion relations (47),

$$\delta n_{1,2} \propto \int_{-\infty}^{\infty} \delta \tilde{n}_{1,2}(p) e^{i[py - \omega_{1,2}(p)t]} dp. \quad (48)$$

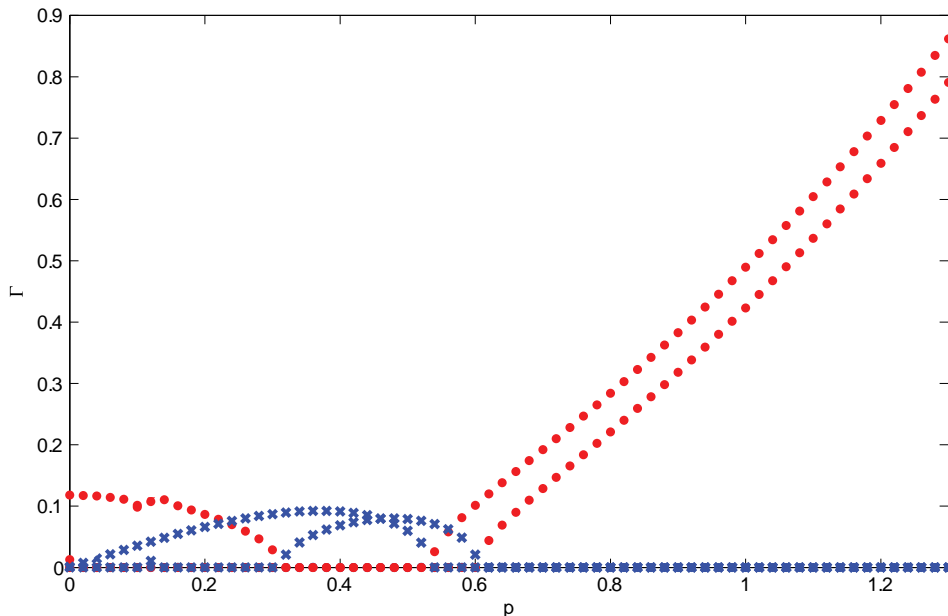


FIG. 5: (Color online.) Two branches of dispersion curves $\Gamma(p)$ for unstable disturbances around the dark-soliton solution. Real parts of Γ are shown by crosses, and imaginary parts by dots. Parameters are $g_{11} = 1, g_{22} = 1.6, g_{12} = 0.1, n_{10} = 1, n_{20} = 0.6$.

This representation implies that the integral is convergent, i.e., the wave packet is finite along coordinate y . Its time dependence at fixed value of y is determined by dispersion relations $\omega_{1,2}(p)$. Since expressions (47) contain imaginary parts, $\delta n_{1,2}$ can grow exponentially with time, which implies instability of the dark soliton, as is well known for the zero flow, $U_s = 0$. However, it may happen that, for U_s large enough, wave packets are carried away so fast that they cannot grow at fixed value of y , which is precisely the transition from absolute to convective instability [30]. Mathematically, the convective instability means that one can transform integrals over p in wave packets (48) into integrals over ω , because these wave packets have finite duration. In other words, function $\omega = \omega(p)$ can be inverted to define single-valued dependence $p = p(\omega)$. Therefore, the distinction between absolute and convective instabilities depends on analytical properties of dispersion relations (47) [30, 31]. Actually, the transition from absolute to convective instability is determined by critical points p_{cr} where $d\omega/dp = 0$, and function $p = p(\omega)$ changes its behavior: at $U_s < (U_s)_{cr}$ it is represented in the complex p plane by disconnected curves, whereas for $U_s > (U_s)_{cr}$ these curves are connected with each other. In the latter case, one can deform the contour of the integration over p , with regard to the single-valuedness of $\omega = \omega(p)$, so as to transform it into an integral over ω . In other words, the spatial Fourier decomposition of the perturbation wave packet can be transformed to a temporal form, which means that the instability is convective.

As is known, the asymptotic behavior of integrals (48) is determined by branching points of function $p = p(\omega)$, where $d\omega/dp = 0$. This yields equation

$$U_s = -i \frac{d\Gamma}{dp}, \quad (49)$$

where, as one can see in Fig. 5, $\Gamma(p, v)$ has either real or purely imaginary values for real p . Therefore, critical values of U_s , at which disconnected contours transform into connected ones, correspond to the appearance of a double root p_{br} of Eq. (49) on the real axis of p . This means $dp_{br}/dU_s = \infty$ at $U_s = (U_s)_{cr}$. The differentiation of Eq. (49) with respect to U_s then leads to equation

$$\left. \frac{d^2\Gamma}{dp^2} \right|_{p=p_{cr}} = 0 \quad (50)$$

for the corresponding critical value, $p_{cr}(v)$. The substitution of that value into Eq. (49) yields function $U_s(v)$. When

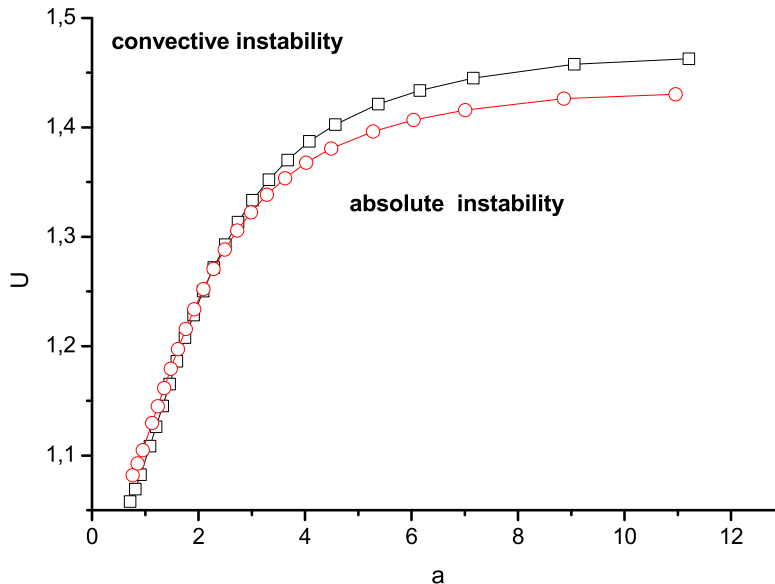


FIG. 6: (Color online.) Curves separating regions of the absolute and convective instabilities of dark solitons in the two-component condensate with parameters $g_{11} = 1$, $g_{22} = 1.6$, $g_{12} = 0.1$, $n_{10} = 1$, $n_{20} = 0.6$. The respective sound velocities are $c_+ = 1.03$, $c_- = 0.95$. Squares and circles refer to two different unstable modes. Below each curve the corresponding mode is absolutely unstable and dark solitons cannot be created by the flow with velocity U less than $U_{cr} \cong 1.5$ for most slopes a . Dark solitons become just convectively unstable (effectively stable) above both curves, that is for $U > u_{cr} \cong 1.5$.

this function is known, we find, with the help of relations

$$v = \frac{U}{\sqrt{1+a^2}}, \quad U_s = U \sin \varphi = \frac{Ua}{\sqrt{1+a^2}} = av, \quad (51)$$

the slope,

$$a_{cr}(v) = \frac{U_s(v)}{v}, \quad (52)$$

and velocity,

$$U(v) = v\sqrt{1+a_{cr}^2(v)}, \quad (53)$$

as functions of v for all values in the interval ($0 < v < c_+$). As a result, we obtain, in a parametric form, the dependence $U(a)$ for the curve separating regions of the absolute and convective instabilities. Two such curves for both branches are shown in Fig. 6, where the region of the convective instability is located above both curves. It is seen that the dark solitons with large slopes a undergo the transition to the convective instability at flow velocities greater than $U_{cr} \approx 1.5$, as suggested also by the numerical findings reported above.

V. CONCLUSION

In this work, we have considered the effect of dragging a supercritical obstacle through a two-component Bose-Einstein condensate, which was motivated by a number of recent experiments in such settings, predominantly examining the dynamics of mixtures of hyperfine states of ^{87}Rb . The presence of two speeds of sound in the mixture results in the existence of two Mach cones. The motion of the obstacle, in turn, produces two main features, namely, the linear “ship waves” and the oblique dark solitons. For the former pattern, we have developed a description of their density oscillations, which occur outside the Mach cones, in good agreement with numerical findings. On the other

hand, for the dark solitons we have developed an analytical description of their profile, which was also found to be in good agreement with numerical observations. In particular, it was predicted that the dark solitons are confined to the area inside the outer Mach cone, which was confirmed by the simulations.

This work may be a relevant starting point towards a more detailed understanding of the interplay between the inter-species interactions and the loss of superfluidity caused by the super-critical motion of defects. Among natural extensions of the present setting, there may be the consideration of the three-dimensional context, with *vortex rings* being formed as a result of the motion of the obstacle [which is closest to the experimental settings of reported in Refs. [2, 3]]. Another possibility would be to consider the supercritical motion of the obstacle in a three-component spinor mixture [47], where it would be relevant to examine the role of the spin-dependent and spin-independent parts of the interatomic interactions in producing patterns such as those considered herein. Such studies are currently in progress and will be reported in future works.

Acknowledgments

We appreciate a valuable discussion with L.P.Pitaevskii. Yu.G.G. and A.M.K. thank RFFI (Russia) for financial support. P.G.K. gratefully acknowledges support from NSF-CAREER, NSF-DMS-0619492 and NSF-DMS-0806762, as well as from the Alexander von Humboldt Foundation. The work of D.J.F. was partially supported by the Special Research Account of the University of Athens.

-
- [1] L.P. Pitaevskii and S. Stringari, *Bose-Einstein Condensation*, Cambridge University Press, Cambridge, 2003.
 - [2] P. Engels and C. Atherton, *Phys. Rev. Lett.* **99**, 160405 (2007).
 - [3] J.J. Chang, P. Engels and M.A. Hoefer, arXiv:0803.2535.
 - [4] V. Hakim, *Phys. Rev. E* **55**, 2835 (1997).
 - [5] R. Carretero-González, P.G. Kevrekidis, D.J. Frantzeskakis, B.A. Malomed, S. Nandi, A.R. Bishop, *Math. Comp. Simul.* **74**, 361 (2007).
 - [6] G.E. Astrakharchik and L.P. Pitaevskii, *Phys. Rev. A* **70**, 013608 (2004).
 - [7] I. Carusotto, S.X. Hu, L.A. Collins, and A. Smerzi, *Phys. Rev. Lett.* **97**, 260403 (2006).
 - [8] Yu.G. Gladush, G.A. El, A. Gammal, A.M. Kamchatnov, *Phys. Rev. A* **75**, 033619 (2007).
 - [9] Yu.G. Gladush and A.M. Kamchatnov, *Zh. Eksp. Teor. Fiz.* **132**, 589 (2007) [*JETP*, **105**, 520 (2007)].
 - [10] Yu.G. Gladush, L.A. Smirnov, and A.M. Kamchatnov, *J. Phys. B* **41**, 165301 (2008).
 - [11] G.A. El and A.M. Kamchatnov, *Phys. Lett. A* **350**, 192 (2006); erratum: *Phys. Lett. A* **352**, 554 (2006).
 - [12] G.A. El, A. Gammal, and A.M. Kamchatnov, *Phys. Rev. Lett.* **97**, 180405 (2006)
 - [13] G.A. El, Yu.G. Gladush, and A.M. Kamchatnov, *J. Phys. A: Math. Theor.* **40**, 611 (2007).
 - [14] A.M. Kamchatnov and L.P. Pitaevskii, *Phys. Rev. Lett.* **100**, 160402 (2008).
 - [15] E.A. Cornell, report at *Conference on Nonlinear Waves, Integrable Systems and their Applications* (Colorado Springs, 2005); <http://jilawwww.colorado.edu/bec/papers.html>.
 - [16] B. Damski, *Phys. Rev. A* **69**, 043610 (2004).
 - [17] A.M. Kamchatnov, A. Gammal, and R.A. Kraenkel, *Phys. Rev. A* **69**, 063605 (2004).
 - [18] T.P. Simula, P. Engels, I. Coddington, V. Schweikhard, E.A. Cornell, and R.J. Ballagh, *Phys. Rev. Lett.* **94**, 080404 (2005).
 - [19] M.A. Hoefer, M.J. Ablowitz, I. Coddington, E.A. Cornell, P. Engels, and V. Schweikhard, *Phys. Rev. A* **74**, 023623 (2006).
 - [20] R. Carretero-González, P.G. Kevrekidis, D.J. Frantzeskakis, *Nonlinearity* **21**, R139 (2008).
 - [21] W. Wan, S. Jia, and J.W. Fleischer, *Nature Physics*, **3**, 46 (2007).
 - [22] N. Ghofraniha, C. Conti, G. Ruocco, and S. Trillo, *Phys. Rev. Lett.* **99**, 043903 (2007).
 - [23] C. Barsi, W. Wan, C. Sun, and J.W. Fleischer, *Optics Lett.*, **32**, 2930 (2007).
 - [24] S. Jia, W. Wan, and J.W. Fleischer, *Phys. Rev. Lett.* **99**, 223901 (2007).
 - [25] G.A. El, A. Gammal, E.G. Khamis, R.A. Kraenkel, and A.M. Kamchatnov, *Phys. Rev. A* **76**, 053813 (2007).
 - [26] E.G. Khamis, A. Gammal, G.A. El, Yu.G. Gladush, and A.M. Kamchatnov, *Phys. Rev. A* **78**, 013829 (2008).
 - [27] B.B. Kadomtsev and V.I. Petviashvili, *Sov. Phys. Doklady*, **15**, 539 (1970).
 - [28] V.E. Zakharov, *JETP Lett.* **22**, 172 (1975).
 - [29] E.A. Kuznetsov and S.K. Turitsyn, *Sov. Phys. JETP*, **67**, 1583 (1988).
 - [30] E.M. Lifshitz and L.P. Pitaevskii, *Physical Kinetics*, (Pergamon, London, 1981).
 - [31] P. A. Sturrock, *Phys. Rev.* **112**, 1488 (1958).
 - [32] C.J. Myatt, E.A. Burt, R.W. Ghrist, E.A. Cornell and C.E. Wieman, *Phys. Rev. Lett.* **78**, 586 (1997).
 - [33] D.S. Hall, M.R. Matthews, J.R. Ensher, C.E. Wieman and E.A. Cornell, *Phys. Rev. Lett.* **81**, 1539 (1998).
 - [34] D.M. Stamper-Kurn, M.R. Andreas, A.P. Chikkatur, S. Inouye, H.-J. Miesner, J. Stenger and W. Ketterle, *Phys. Rev. Lett.* **80**, 2027 (1998).

- [35] M. Trippenbach, K. Goral, K. Rzazewski, B. Malomed and Y.B. Band, *J. Phys. B* **33**, 4017 (2000).
- [36] I.M. Merhasin, B.A. Malomed and R. Driben, *J. Phys. B* **38**, 877 (2005).
- [37] K. Kasamatsu, and M. Tsubota, *Phys. Rev. A* **74**, 013617 (2006).
- [38] K. M. Mertes, J. W. Merrill, R. Carretero-González, D. J. Frantzeskakis, P. G. Kevrekidis, and D. S. Hall, *Phys. Rev. Lett.* **99**, 190402 (2007).
- [39] V. Schweikhard, I. Coddington, P. Engels, S. Tung, and E.A. Cornell, *Phys. Rev. Lett.* **93**, 210403 (2004).
- [40] H.-J. Miesner, D.M. Stamper-Kurn, J. Stenger, S. Inouye, A.P. Chikkatur and W. Ketterle, *Phys. Rev. Lett.* **82**, 2228 (1999).
- [41] J. Stenger, S. Inouye, D.M. Stamper-Kurn, H.-J. Miesner, A.P. Chikkatur and W. Ketterle, *Nature* **396**, 345 (1999).
- [42] D.M. Stamper-Kurn, M.R. Andrews, A.P. Chikkatur, S. Inouye, H.-J. Miesner, J. Stenger, and W. Ketterle, *Phys. Rev. Lett.* **80**, 2027 (1998).
- [43] M.-S. Chang, C.D. Hamley, M.D. Barrett, J.A. Sauer, K.M. Fortier, W. Zhang, L. You, and M.S. Chapman, *Phys. Rev. Lett.* **92**, 140403 (2004).
- [44] D.M. Stamper-Kurn and W. Ketterle, e-print cond-mat/0005001.
- [45] H. Susanto, P.G. Kevrekidis, R. Carretero-González, B.A. Malomed, D.J. Frantzeskakis and A.R. Bishop, *Phys. Rev. A* **75**, 055601 (2007).
- [46] P.G. Kevrekidis and D.J. Frantzeskakis, *Mod. Phys. Lett. B* **18**, 173 (2004).
- [47] B.J. Dabrowska-Wüster, E.A. Ostrovskaya, T.J. Alexander and Yu.S. Kivshar, *Phys. Rev. A* **75**, 023617 (2007).